COBEM 2023 27TH INTERNATIONAL CONGRESS OF MECHANICAL ENGINEERING

ABCM Brazilian Society of Mechanical Sciences and Engineering
27th ABCM International Congress of Mechanical Engineering
December 04-08, 2023, Florianópolis-SC, Brazil

COBEM2023-1089
Investigating the Parameters of a Spar Model Platform through Still Water Decay Tests Using Low-Cost IMU Readings

Aline Leal de Lima Gontarski
Department of Naval and Oceanic Engineering, Polytechnic School of the University of São Paulo
aline.peresleal@usp.br
Igor Rosa Ferreira Gomes[2]
I.igor.gomes@grad.ufsc.br
Ana Luiza Reigota Lira[2]
ana.luiza.r.lira@grad.ufsc.br
André Luís Condino Fujarra [2]
andre.fujarra@ufsc.br
[2]Technical Centre of Joinville, Federal University of Santa Catarina

Abstract. *Offshore structures as platforms for gas production or wind turbines undergo flow-induced motions (FIM) since they are exposed to wind forces, currents and waves, leading to considerable motion amplitudes. FIM refers to the motion of a structure caused by the fluid flow forces acting on it. Vortex-induced motion (VIM), on the other hand, is a specific type of FIM that is caused by the vortices shedding in the fluid flow. This phenomenon generates unsteady forces on the structure that leads it to oscillate mainly in cross-flow and in-line directions. To reduce movement during platform operation, the design phase must take into account the natural frequencies of the structure. Water decay tests are usually used to determine the parameters of the structure in this environment. In this work, an scaled platform model was built to conduct still water decay tests using a low-cost inertial measurement unit (IMU) to record data. The model was built based on tests that had already been conducted by the authors at University of Tokyo (UTokyo), to evaluate the VIM response of the platform. The objective is to investigate the behavior of the platform and to validate the precision of data acquisition from two Inertial Measurement Units (IMUs). The process of converting acceleration and rotation rates into displacement in a specific frame using a low-cost IMU can potentially lower the cost of laboratory dynamic analysis. The experimental setup and calibration method are detailed in the work. A data treatment process employing Kalman filter and intrinsic mode functions (IMF) is described, followed by the signal analysis to find natural frequencies and displacement time history. The results are analyzed and discussed, comparing them to an optical tracking system. The results highlight the potential of IMUs as a reliable and cost-effective tool for collecting data in still water decay tests. Overall, this study contributes to the understanding of the behavior of spar platforms design and provides expertise to built and carry out model tests for such structures.*
Keywords: *VIM, platform model, still water decay test, inertial sensors, IMU*

1. INTRODUCTION

The offshore wind energy industry and gas production continues to expand into deeper water, where spar platforms have become an increasingly popular choice. These structures are exposed to extreme environmental loads which can induce significant forces and moments on the structure. These loads may damage the structure, leading to fatigue and even catastrophic failure if not taken into account during the design phase. Moreover, the interaction between different components of the offshore system, such as the platform, mooring system, and risers, affects the behavior of the structure. Thus, a thorough understanding of offshore structures' behavior is crucial to ensure safe and reliable offshore facilities. This can be achieved by using a combination of numerical simulations, laboratory experiments, and field measurements to optimize their design and operation.

Numerical simulations and laboratory experiments regarding a monocolumn platform have been conducted in the last years (Çelik and Altunkaynak, 2020; Leroy *et al.*, 2022; Fujarra *et al.*, 2022, 2023). Çelik and Altunkaynak (2020) investigated the hydrodynamic parameters of a fixed oscillating water column (OWC) device using physical experiments and 3D numerical simulations. The damping ratio, natural and resonant frequencies, and added mass were analyzed for several configurations. The findings include a new empirical equation for the natural frequency and valuable insights for optimizing OWC performance, estimating the system's response to wave excitation. In the study of Fujarra *et al.* (2022) the influence of initial roll and pitch angles on the vortex-induced motion (VIM) amplitudes of a floating circular cylinder with a low aspect ratio was investigated. Four different initial angle conditions were tested and the experiments were conducted in a towing tank, using a model with 6 degrees of freedom (6DOF) and an optical tracking system to acquire motion data. Reduced velocities ranged from $1 \leq Vr \leq 12$, and the Reynolds number range performed was

$12,000 \leq Re \leq 100,000$. The results indicated that the initial pitch angles played a significant role in promoting yaw motions, resulting in geometric asymmetry of the body and increased VIM amplitudes. Yaw motions became substantial when the mean pitch angle of the cylinder exceeded three degrees. The study emphasized the importance of accurately modeling and analyzing yaw motions in the context of vortex-induced motions on floating offshore wind turbines (FOWT) to ensure reliable estimation of fatigue life and operational downtime of the mooring systems. In the paper of Leroy *et al.* (2022), they have investigated the hydro-elastic response of a large floating wind turbine in both regular waves and severe sea-states. The experimental model replicates the turbine's behavior by incorporating a flexible backbone and lightweight floaters with scaled geometry. Tri-axial accelerometers were employed to measure accelerations at the wind turbine, platform top, and platform bottom. The motion of the model was tracked using a Qualysis optical tracking system, capturing the tower top and platform top's six degrees of freedom. Additionally, an inertial measurement unit (IMU) measured roll and pitch rotations at the platform bottom. Decay tests were conducted to identify the natural periods of the rigid degrees of freedom, while hammer tests were used to verify the targeted bending mode period. The experimental data highlight the significance of considering nonlinear hydrodynamics when analyzing the turbine's behavior. Fujarra *et al.* (2023) studied the development of a low-cost solution for accurately predicting displacements and frequencies of offshore structures using an inertial measurement unit (IMU) and signal treatment techniques. Two experimental studies were conducted, including decay tests on a vertically clamped cylinder in air and decay tests on a spar platform model in a water tank. To validate the results obtained from an inertial measurement unit (IMU), different positions and initial excitations were tested. Signal treatment techniques, such as applying a Kalman filter to extract IMU angles and using quaternion rotation, were employed. Additionally, Fourier filtering, trapezoidal integration, and intrinsic mode function (IMF) drift removal were used to address noise and drift issues. The IMU results for frequencies and displacement time histories were compared with an optical tracking system, and the average relative error was found to be less than 2.8% for both air and water decay tests.

Field measurements, otherwise, are less commonly found in the literature, as the costs of such measurements are still very high. Field monitoring usually involves robots, such as autonomous underwater vehicles (AUV) cited by Wang *et al.* (2018).

Inertial measurement units (IMUs) are devices that measure accelerations and angular rates in three dimensions, and can be used to calculate the orientation and displacement of an object. They are used in a variety of applications, including navigation and control of vehicles, drones, and robots, as well as in virtual reality and augmented reality systems. Their small size, light weight, and ability to operate autonomously make them a good alternative to use in offshore environments. The usage of IMUs can provide significant cost savings by reducing the need for expensive and complex instrumentation.

In this context, this work aims to investigate the modal parameters of a spar model platform in reduced scale using low-cost IMU readings. The water decay tests were conducted in a controlled laboratory environment, where the spar model was subjected to different initial displacements to excite its six degrees of freedom. An optical tracking system was used to validate the low-cost IMU motion results, showing the reliability of the displacement and angles calculated through the proposed method. The main goal is to show how IMUs can be used to obtain reliable data from experimental water tests, even for different initial position, displacement scales or different inertial sensors set.

2. EXPERIMENTAL SETUP

The experiments were conducted in a still water tank at the Laboratory of Fluid-Structure Interaction at Federal University of Santa Catarina (UFSC). A spar platform model was built, made of five different parts following described (see Fig. 1):

- Deck: which was designed and 3D printed with the purpose of placing the IMU, serving as support for the springs that connect the model to the external structure, and supporting the internal structure;
- Internal structure: which allows modification of the model's CG by changing the height of its metal ballast using a 6mm diameter threaded rod;
- Column: with an external diameter of 50mm, 2mm thick walls, and a total length of 435mm;
- Bottom: with the purpose of making the platform body watertight and supporting the internal structure;
- Springs: fixed to an external structure and connected to the deck, the springs allow the model to reach its natural frequency, given the model stiffness.

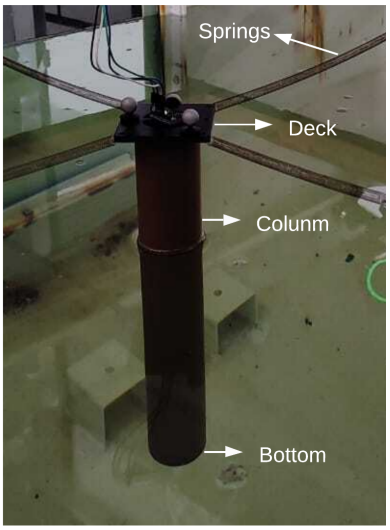

Figure 1. Spar scaled model.

Table 1. Model parameters.

	Value	Unit
D	50.0	mm
L_{sub}	338 .4	mm
L/D	6.8	
L_t	435.5	mm
B_{tank}	1200.0	mm
blockage	4.2	%
CG (from the bottom)	135.8	mm
CB (from the bottom)	169.2	mm
$CB - CG$	33.3	
mass	663.0	g
∇	663.0	g

The springs were chosen according to the natural frequency desired for the model in the sway direction ($f_{n,y}$), which is 0.1Hz. The natural frequency was calculated by Eq. 1,

$$f_{n,y} = \frac{1}{2\pi}\sqrt{\frac{k}{(m+m_a)}} \tag{1}$$

where k is the spring set stiffness, m is the structural mass, m_a is the added mass. With that, the springs were designed through the following equation:

$$k = \frac{d_s^4 G}{8 D_s^3 N_a} \tag{2}$$

where d_s is the wire diameter, D_s is coil diameter, G is the elastic modulus and N_a is the number of active turns. Stainless steel 302 was chosen as the material of the springs.

A summary of the spar scaled model parameters is presented in Tab.1. The scale factor is $1:340$ related to the real scale platform, which has a diameter of 17 m.

Finally, to build the external structure that holds the platform centralized in the hydrostatic tank, two wooden beams with dimensions of 40x40x1000mm (height x width x length) and two beams of 40x40x1200mm were used, forming a quadrilateral structure centered in relation to the internal walls of the tank (see Fig.2).

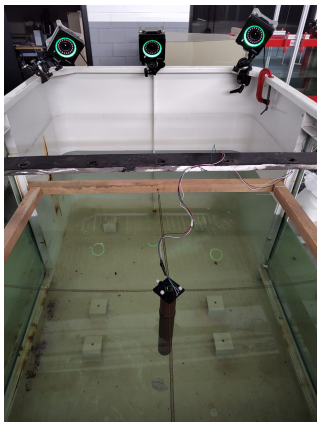

Figure 2. Experimental setup.

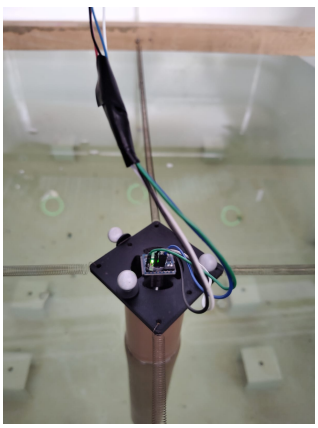

Figure 3. IMU and reflective targets placed on the model deck.

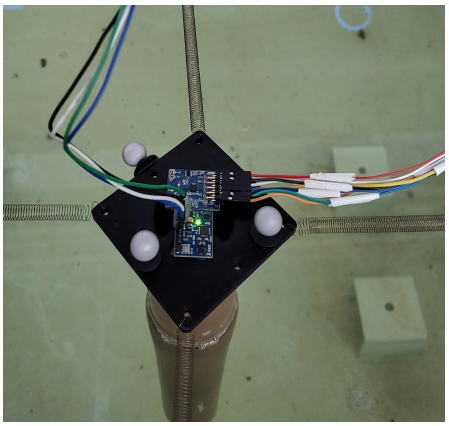

Figure 4. Two IMUs placed on the model.

Related to the data acquisition tools, a low-cost MEMS-based Inertial Measurement Unit (IMU) was used to monitor the motion of the body in our experiments.

The term "low cost" is often used to describe both consumer-grade and tactical-grade sensors, which are not accurate enough without treatment and usually need to be fused with other kinds of sensors, according to Groves (2013). The sensors used in this work cost about $10,00 and $40,00 for the GY-87 and PmodNAV, respectively.

The IMU consists of accelerometers, gyroscopes, and magnetometers sensors, which measure the body's acceleration, angular velocity, and orientation in space. By attaching the IMU to the model, as can be seen in Fig.3, we have obtained motion and rotations data. It is important to note that IMUs can be susceptible to drift and inherent errors over time. Solving this problem is possible with proper signal treatment, described in Sec.3.

In addition to the IMU, we have incorporated OptiTrack, an optical tracking system, to meticulously monitor the displacement of a rigid body and validate the IMU results. The system comprises three cameras placed on the tank walls, as shown in Fig. 2, that captured the motion of reflective markers affixed to the model deck. The Motive, a motion capture software developed by OptiTrack, was employed to calibrate the tracking system, set the coordinate frame, configure the camera setup, define the tracking parameter and record data at a sampling frequency of 100 Hz. This enabled us to obtain precise 6DOF motion data throughout the experiments, to compare to the measurements obtained from the IMU.

Additionally, to demonstrate the reliability of the signal treatment process adopted, we have rotated the IMU GY-87 and included a second IMU in our study, called PmodNAV. By utilizing two separate IMUs, each with its own set of accelerometers, gyroscopes, and magnetometers, we aimed to compare and validate the motion data obtained from both sensors. The setup with two IMUs is illustrated in Fig.4.

3. DATA ANALYSIS

The post-processing analysis of the data was performed using Octave software. To extract useful information from the raw data, a series of steps were applied in the signal analysis methodology.

The calibration of the accelerometers was done with multiposition calibration proposed by Zhang *et al.* (2008). The magnetometer calibration involves aligning it properly and compensating for any external magnetic interference, calculating soft and hard iron errors that deform the Earth magnetic field. Lastly, to find the rate gyros gain, a Computer Numerical Control (CNC) machine was used, where with a defined rotation velocity, the readings from the IMU were calibrated. Rate gyros offsets were find with an static test.

The coordinate frames adopted are defined as follows: the reference frame, illustrated by the blue axis in Fig. 5, is fixed and composed by the X-axis pointing towards the north, the Y-axis points towards the east, and the Z-axis points directly downward. The object frame, illustrated by the green axis in Fig. 5, moves with the object (i.e. IMU) and the axes points to the direction of movement. Euler rotations describe the orientation of the object frame (xyz) with respect to the reference frame (XYZ). Then, Euler's angles are represented in this work by the angles roll (ϕ), pitch (θ) and yaw (ψ). The optical tracking system frame was placed according to the reference frame.

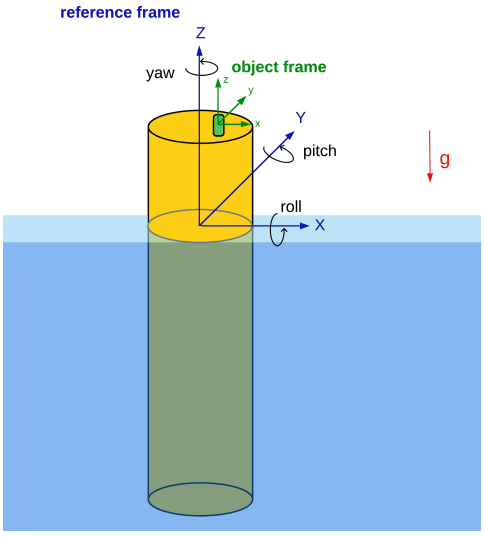

Figure 5. Object and reference frames illustrated in the spar model.

The initial angles related to XYZ frame were computed from the static test. Angle initialization was done by the accelerometer and magnetometer sensors, following the Eqs. 3, 4 and 5 (Groves, 2013; Peres and Fujarra, 2021):

$$\phi = atan2\left(-a_y, -a_z\right); \tag{3}$$

$$\theta = atan2\left(a_x, \sqrt{a_y^2 + a_z^2}\right); \tag{4}$$

$$\psi = atan2\left(M_Y, M_X\right); \tag{5}$$

being:

$$\begin{aligned} M_Y =& - m_y cos\phi + m_z sin\phi \\ M_X =& m_x cos\theta + m_y sin\phi sin\theta + m_z cos\phi sin\theta \end{aligned} \tag{6}$$

where a_x, a_y and a_z are the accelerations and m_x, m_y and m_z are the magnetometer readings on the axis x, y and z of the object frame, respectively.

After that, Euler angles were calculated with Kalman Filter, to filter out noise and drifts. Angles from the Eqs. 3, 4 and 5 as well as from the rate gyros integration were employed. Quaternions (q) were built with those Euler angles and the rotation of the acceleration vector (a) was made for every time step, using Eq. 7.

$$a' = qaq^* \tag{7}$$

where q^* is the complex conjugate of q. The rotated coordinates from a' are extracted from its imaginary part.

Empirical Mode Decomposition (EMD) is a data analysis technique used to break down a complex signal into a finite set of oscillatory components called Intrinsic Mode Functions (IMFs). Each IMF represents a different scale or frequency component of the original signal, and they are derived through an iterative sifting process (Huang *et al.*, 1998). Accordingly, before time integration process, low frequencies were filtered out using the trend estimation by IMFs. Trapezoidal method was used for the integration process and, the drift coming from the integration process was removed using the residual signal estimated by IMFs one more time. The same process was conducted with velocity integration to find out displacements over time.

Finally, the displacement vector was rotated to the initial angles computed, to compare the components with the signal obtained by the optical system.

Natural frequencies were estimated by Fourier analysis, where the Nyquist frequency was observed during the tests. The peak frequency is related to the degree of freedom excited in the test. When more than one frequency was identified in the frequencies spectra, it becomes crucial to determine the specific component of interest.

The Fourier filter can also be used to isolate the amplitudes associated with the frequency of interest, effectively removing unwanted frequency components. Having the signal from a single DOF, damping factor (ζ) is calculated by logarithmic decrement, as follows (Rao, 2001):

$$\zeta = \frac{\delta}{\sqrt{4\pi^2 + \delta^2}} \tag{8}$$

where δ is given by the logarithmic decrement, which means $\delta = log\left(x_n / x_{n+1}\right)$. The equation for the envelope in the logarithmic decrement method is approximated by:

$$A(t) = A(0)exp(-\zeta\omega_n t) \tag{9}$$

where $A(t)$ is the displacement amplitude as a function of time and, ω_n is the structure natural frequency in rad/s.

The signal processing flow chart shown in Fig. 6 is a visual representation of the methodology employed for data analysis and manipulation. This diagram outlines the sequential steps involved in the signal processing, from initial data acquisition through the accelerometers, magnetometers and rate gyros sensors, passing by Kalman filter, quaternion rotation, time integration and IMF trend removal; to the final output generation: displacements and rotations in a desired frame of reference. The flow chart not only facilitates a clearer understanding of the signal processing workflow but also serves as a valuable reference for those seeking to replicate the study.

4. RESULTS AND DISCUSSIONS

In this section, we present the results of our study on the behavior of a spar model platform under still water decay tests calculated by inertial sensors. The results include its natural frequencies, damping ratios, and displacement and rotation time-histories.

Starting with the calibration, for the accelerometers, the rotation matrix and offset values were computed. For the rate gyros, offsets were estimated having the IMUs in a static position. These results can be seen in Fig. 7, where a normal

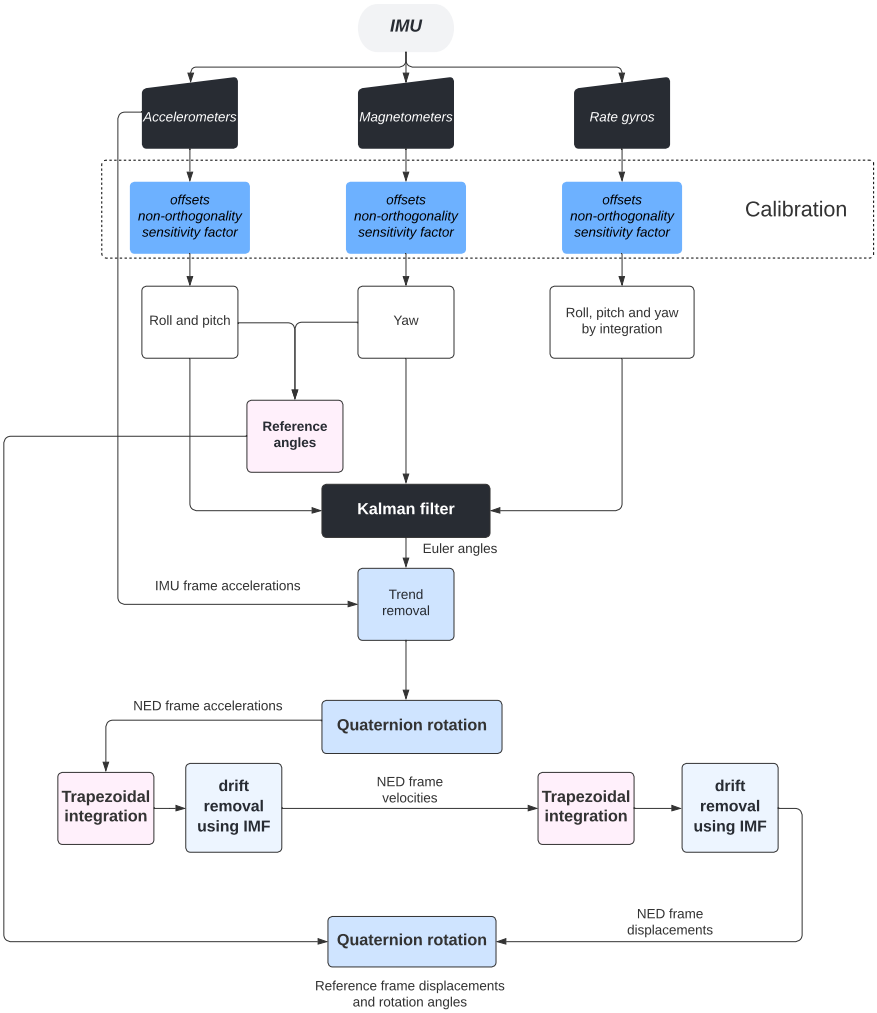

Figure 6. IMU signal processing flow chart.

distribution of values is observed, and for the calibrated data, a zero-centered histogram. In Fig. 8 the magnetometers values are presented in two sets: raw values (shown in magenta) and calibrated data (presented in green). The calibrated data points are fitted with a zero-centered sphere.

As explained in the Sec. 3, the displacement was obtained by double integration of the accelerometers values, properly rotated to a fixed reference frame. It was noted that one important step to ensure a reliable integration process is to cut the signal to be integrated at one of its peak values (point of inflection). By doing so, the result of the integration will start from zero, which is in accordance with the *cumtrapz* algorithm. That helps eliminate any potential integration errors that may arise from the initial condition. Figure 9 presents one example of signal obtained by the integration process and residue removal. It's noticed how the noise decreases after these steps.

Regarding the trend estimation and drift removal, when compared to the last work of the authors Fujarra *et al.* (2023), in the present work it was observed how the detrending process covers more than just the last IMF. Mainly in signal passing through time integration, as in here, noises increase the signal amplitude and the energies of the IMFs need to be estimated to filter out noises from the signal components, according to the work of Patrick Flandrin *et al.* (2004). For this, it is necessary the analyst evaluation of the functions corresponding to the real signal. One example of IMFs obtained from the integrated data is shown in Fig. 10

Evaluating the displacement results from the decay tests, the surge motion was coupled with pitch rotation, while sway was coupled with roll. This configuration is illustrated in Fig.11, where the optical tracking system displacement results are shown in blue, and the IMU GY-87 results are shown in red. Although the initial displacement was imposed in the X direction, the degrees of freedom were coupled during the free movement.

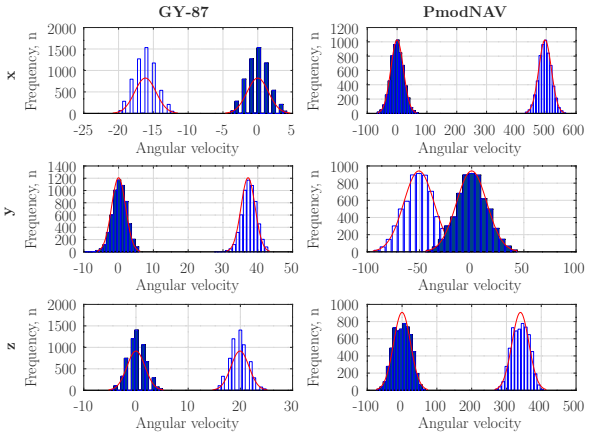

Figure 7. Rate gyros calibration results. Raw data shown in the contour bars and calibrated data in filled bars.

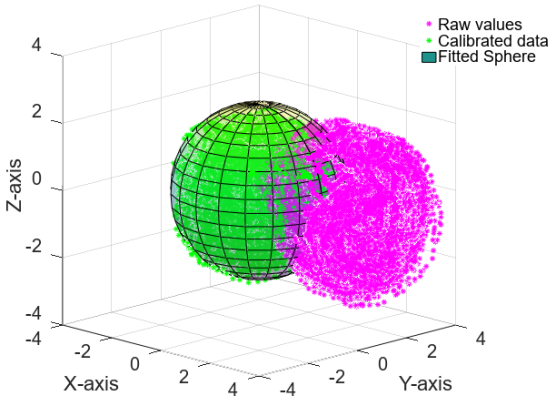

Figure 8. Magnetometers values calibration for GY-87.

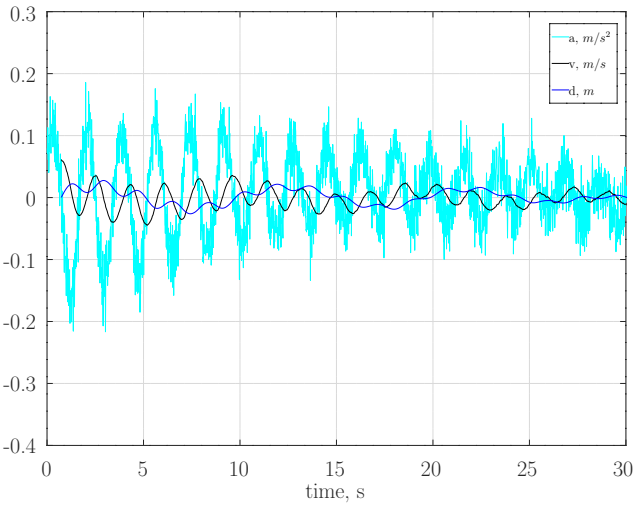

Figure 9. Acceleration (cyan), velocity (black) and displacement (blue) obtained through time integration and residue removal.

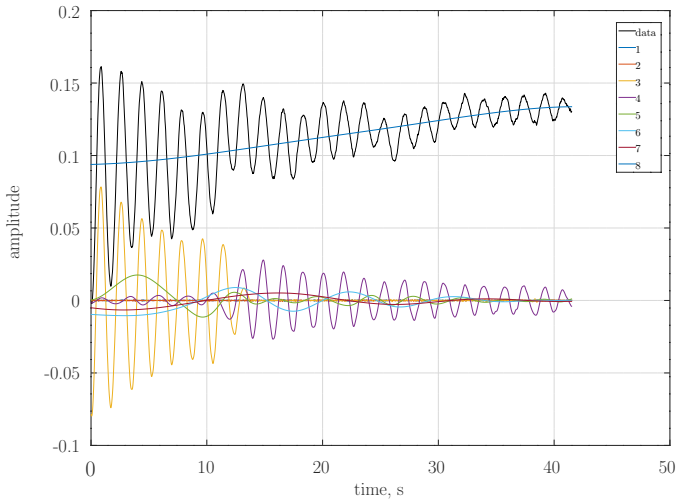

Figure 10. Empirical Mode Decomposition: original signal in black and its Intrinsic Mode Functions (IMFs).

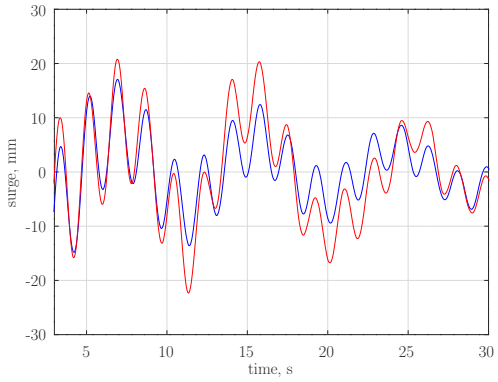

Figure 11. Surge motion (low frequency) coupled with pitch rotation (high frequency). IMU results in red and Optitrack in blue.

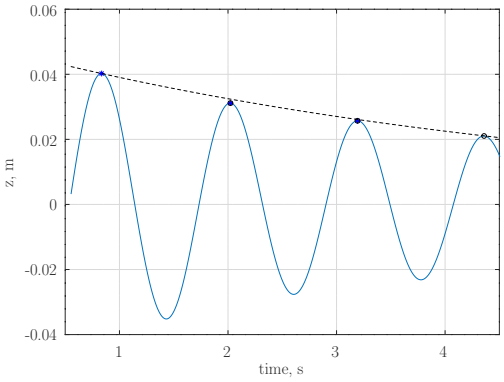

Figure 12. Heave logarithmic decrement, $\zeta = 0.034$ for IMU and $\zeta = 0.032$ for optical tracking.

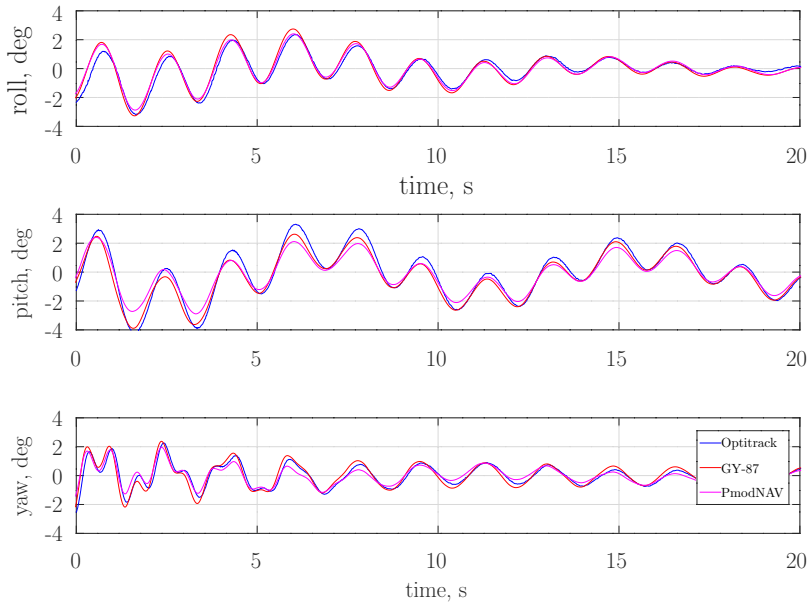

Figure 13. Rotation angles from the two inertial measurements system sets and the optical tracking system.

Other point observed in this work is that when the rotation in roll and pitch are relevant, the computation of yaw angles using magnetometers is not consistent, as described in Groves (2013) and confirmed by the present experiments. In this way, as the trend estimated by last IMFs is useful to remove drift from the integration process, the magnetometer was only used to estimate the initial orientation angle. The yaw angle over time was calculated by the rotation rate integration, and its last IMF was used to correct the drift.

The angles strongly influence the displacement computation, since the small disturbance during the rotation affects the acceleration amplitudes in the fixed frame, and, this difference is amplified in the double integration process.

The natural damped frequencies obtained during the decay tests are presented in the Tab. 2. Relative errors (e) between the two systems are small, as well as the standard deviation (σ) among tests. The surge and sway motions, due to their lower frequencies, also exhibit relatively larger errors, but these errors do not exceed 6.5%.

Compared to the model built and tested at Utokyo by Fujarra *et al.* (2023), shown in Tab. 3, despite the different constructions, the models exhibited qualitatively similar natural frequencies, except for the heave frequency due to their geometric properties ($k_6 = A_w h \rho g$).

Related to the damping factor, decay displacements for heave motion are illustrated in Fig. 12, where it is observed the logarithmic decrement in the peak amplitudes and the fitted envelope (dashed line).

In Fig. 13 the angles obtained with the optical tracking system and both IMUs are illustrated over 20 seconds of acquisition. It is possible to conclude how coherent are the results of a system which costs less than a hundred dollars

Table 2. Tests natural frequencies and their mean values, for the inertial measurement unit (IMU) and optical tracking system.

DOF	test	f_{IMU} [Hz]	$\overline{f_{IMU}}$ [Hz]	σ [Hz]	f_{OPTI} [Hz]	$\overline{f_{OPTI}}$ [Hz]	σ [Hz]	e [%]
surge	1	0.116			0.117			
surge	2	0.119	0.117	0.002	0.107	0.110	0.005	-5.83%
surge	3	0.117			0.110			
sway	1	0.102			0.113			
sway	2	0.111	0.106	0.004	0.113	0.113	0.001	6.29%
sway	3	0.106			0.112			
heave	1	0.848			0.848			
heave	2	0.849	0.849	0.003	0.843	0.846	0.003	-0.38%
heave	3	0.854			0.846			
roll	1	0.564			0.562			
roll	2	0.561	0.561	0.002	0.566	0.562	0.007	0.13%
roll	3	0.560			0.553			
pitch	1	0.569			0.561			
pitch	2	0.555	0.557	0.007	0.556	0.556	0.004	-0.14%
pitch	3	0.557			0.554			
yaw	1	1.544			1.542			
yaw	2	1.545	1.544	0.005	1.545	1.542	0.012	-0.10%
yaw	3	1.535			1.522			

Table 3. Models natural frequencies.

Fujarra *et al.* (2023) [Hz]	Present [Hz]
0.122	0.117
0.121	0.106
0.527	0.849
0.455	0.561
0.423	0.557
1.545	1.544

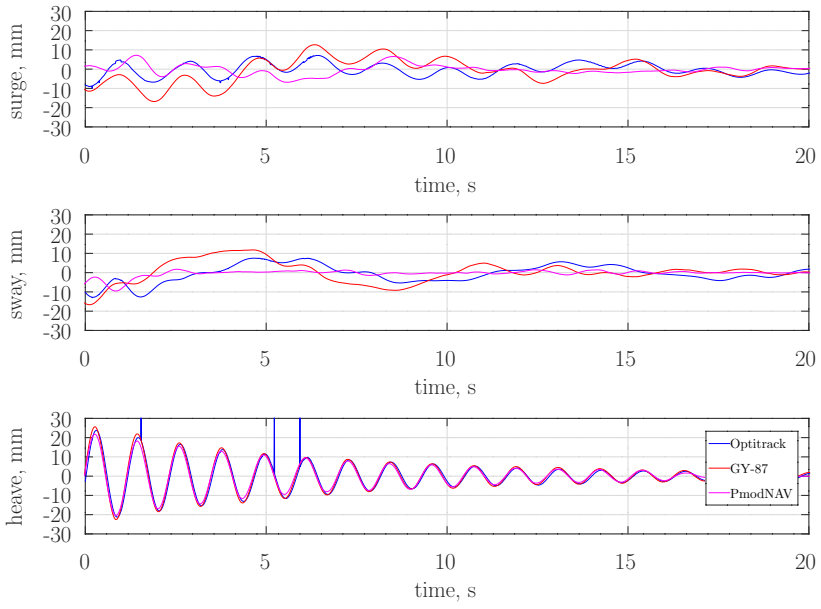

Figure 14. Linear displacements from the two inertial measurements system sets and the optical tracking system.

(IMUs) compared to the one which costs more than tens of thousands of dollars (optical) .

Figure 14 illustrates oscillations occurring in the three directions, i.e. surge, sway and heave. By analyzing the variations in these three dimensions, we can observe the heave movement shows better agreement and this is the moviment initially excited in this test. In the surge and sway directions only two cycles happens in the period evaluated and, the amplitudes are lower. Besides that, it is visible the coupled movement with rotation and translation in those directions. Hence, notable differences in the observed signals become particularly pronounced, and these variances can be justified by the considered periods and the low amplitudes assessed.

5. CONCLUSIONS

In this study, the behavior of spar model in still water decay tests was investigated through low-cost IMUs. A scaled platform model was built for the experimental investigation, based on prior tests conducted by the authors. The results obtained from the IMU data were compared and analyzed in relation to an optical tracking system. It was noted how the angle values can impact the results, being necessary the correct rotation the Earth fixed frame before performing the integration in the signal. Intrinsic Mode Functions are important tools to solve double time integration problems arising from noisy data. The proposed signal processing leads to consistent rigid bodies displacement in a specific frame of reference, even for IMY GY-87 as well for PmodNAV and different initial position. When compared the present model diameter (D=50mm) with the previously tested model(D=172mm), different scales are also covered by the proposed treatment. For decay tests, frequencies are computed with error less than 6.3% , as well as for damping factor. The findings demonstrated that the low-cost IMU could serve as a reliable and cost-effective tool for collecting data in still water decay tests. The accuracy of the IMU measurements was comparable to that of the optical tracking system, indicating its suitability for assessing the behavior of scaled models. The advantage of using the IMUs include low-mass, low-cost, easy installation and transportation. The usage of low-cost IMUs in laboratory testing offers a promising avenue for cost reduction without compromising accuracy in dynamic analysis.

6. ACKNOWLEDGEMENTS

The Coordination of Improvement of Higher Education Personnel (CAPES) is acknowledged by the first author for the PhD scholarship.

7. REFERENCES

Çelik, A. and Altunkaynak, A., 2020. "Determination of hydrodynamic parameters of a fixed owc by performing experimental and numerical free decay tests". *Ocean Engineering*, Vol. 204, p. 106827.

Fujarra, A.L., Cenci, F., Silva, L.S., Hirabayashi, S., Suzuki, H. and Gonçalves, R.T., 2022. "Effect of initial roll or pitch angles on the vortex-induced motions (VIM) of floating circular cylinders with a low aspect ratio". *Ocean Engineering*, Vol. 257, No. May. ISSN 00298018. doi:10.1016/j.oceaneng.2022.111574.

Fujarra, A.L.C., Leal, A.P., Carnier, R.M., Gonçalves, R.T. and Suzuki, H., 2023. "Validation of a low-cost imu for flow-induced vibration tracking in offshore systems". *Journal of the Brazilian Society of Mechanical Sciences and Engineering*, Vol. 45, No. 7, p. 356.

Groves, P., 2013. *Principles of GNSS, Inertial, and Multisensor Integrated Navigation Systems, Second Edition*. GNSS/GPS. Artech House. ISBN 9781608070053. URL `https://books.google.com.br/books?id=t94fAgAAQBAJ`.

Huang, N.E., Shen, Z., Long, S.R., Wu, M.C., Snin, H.H., Zheng, Q., Yen, N.C., Tung, C.C. and Liu, H.H., 1998. "The empirical mode decomposition and the Hubert spectrum for nonlinear and non-stationary time series analysis". *Proceedings of the Royal Society A: Mathematical, Physical and Engineering Sciences*, Vol. 454, No. 1971, pp. 903–995. ISSN 13645021. doi:10.1098/rspa.1998.0193.

Leroy, V., Delacroix, S., Merrien, A., Bachynski-Polić, E. and Gilloteaux, J.C., 2022. "Experimental investigation of the hydro-elastic response of a spar-type floating offshore wind turbine". *Ocean Engineering*, Vol. 255, p. 111430.

Patrick Flandrin, Paulo Gonçalvès and Gabriel Rilling, 2004. "Detrending and denoising with empirical mode decompositions - IEEE Xplore Document". *2004 12th European Signal Processing Conference*, pp. 1581–1584.

Peres, L.A. and Fujarra, A.L.C., 2021. "Signal treatment and analysis of a low cost strapdown inertial measurement unit". In *26th International Congress of Mechanical Engineering*.

Rao, S.S., 2001. *Mechanical vibrations*.

Wang, P., Tian, X., Peng, T. and Luo, Y., 2018. "A review of the state-of-the-art developments in the field monitoring of offshore structures". *Ocean Engineering*, Vol. 147, No. November 2017, pp. 148–164. ISSN 00298018. doi: 10.1016/j.oceaneng.2017.10.014. URL `https://doi.org/10.1016/j.oceaneng.2017.10.014`.

Zhang, H., Wu, Y., Wu, M., Hu, X. and Zha, Y., 2008. "A multi-position calibration algorithm for inertial measurement units". In *AIAA guidance, navigation and control conference and exhibit*. p. 7437.

8. RESPONSIBILITY NOTICE

The authors are solely responsible for the printed material included in this paper.